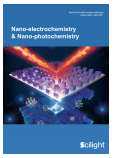
Scilight

Nano-electrochemistry & Nano-photochemistry

https://www.sciltp.com/journals/nenp



Review

Check for updates

Recent Progress in Inorganic Persistent Luminescence Nanoparticles for Sensing and Detection

Meng Cui, Yiming Ma and Lingling Li *

Department of Pharmaceutics, School of Pharmacy, Nanjing Medical University, Nanjing 211166, China
* Correspondence: lill@njmu.edu.cn

How To Cite: Cui, M.; Ma, Y.; Li, L. Recent Progress in Inorganic Persistent Luminescence Nanoparticles for Sensing and Detection. *Nano-electrochemistry & Nano-photochemistry* **2026**, *2*(4), 25. https://doi.org/10.53941/nenp.2026.100025

Received: 26 June 2026
Revised: 10 October 2026
Accepted: 20 October 2026
Published: 13 November 2026

Abstract: Persistent luminescence nanoparticles (PLNPs) are a class of functional nanomaterials capable of storing external excitation energy and continuously releasing photons after excitation stops. Compared with organic persistent luminescence materials, inorganic systems (InPLNPs) have prominent advantages including high luminescence brightness, long afterglow life, good chemical stability and strong photobleaching resistance. Combined with their core characteristics such as no need for in-situ excitation, minimal autofluorescence background and high signal-to-noise ratio, they provide a new technical approach for trace target detection in complex systems, demonstrating significant application value in clinical diagnosis, environmental monitoring, food safety and other fields. This review systematically summarizes the classification, synthesis and surface functionalization methods, persistent luminescence mechanisms and performance regulation strategies of InPLNPs, generalizes the construction strategies of InPLNP-based sensing systems, highlights their application progress in various target detections, and finally discusses the challenges and future development directions in this field.

Keywords: persistent luminescence nanomaterials; persistent luminescence; excitation-free sensing; biosensing; optical detection

1. Introduction

Optical sensing technology plays an irreplaceable role in food safety testing, environmental monitoring, clinical diagnosis, and biomedical research owing to its advantages of high sensitivity, rapid response, and in-situ non-destructive detection capability. However, conventional fluorescence sensing relies on real-time excitation by external light sources, which inevitably causes autofluorescence interference from endogenous fluorophores (e.g., flavoproteins, NADPH, collagen) in complex matrices, severely reducing the signal-to-noise ratio and detection sensitivity. Furthermore, issues such as excitation light scattering and probe photobleaching further restrict the application of conventional fluorescence sensing in complex matrices [1,2].

The emergence of persistent luminescence nanoparticles (PLNPs) offers a new approach to overcoming these bottlenecks. These materials have unique electron storage and release mechanisms, whereby energy from excitation sources such as ultraviolet, visible light, and X-rays is stored in trap energy levels formed by lattice defects. After excitation ceases, trapped carriers are slowly released to produce sustained luminescence, which is known as persistent luminescence (PersL) [3,4]. The most prominent advantage of PLNPs is their in-situ excitation-free feature, where the excitation and emission processes are temporally separated and can continue to glow for seconds or even days after excitation stops [5,6]. Therefore, collecting PersL signals after excitation termination effectively avoids autofluorescence and light scattering interference generated by biological tissues and complex substrates under excitation light irradiation, thereby significantly improving the signal-to-noise ratio (SNR) and detection sensitivity. This unique advantage makes PLNPs highly promising optical probes in the sensing field.

Copyright: © 2026 by the authors. This is an open access article under the terms and conditions of the Creative Commons Attribution (CC BY) license (https://creativecommons.org/licenses/by/4.0/).
Publisher's Note: Scilight stays neutral with regard to jurisdictional claims in published maps and institutional affiliations.

The PersL phenomenon was discovered and utilized by humans as early as the 17th century [7], but it was not until the late 20th and early 21st centuries, with the development of nanosynthesis techniques, that researchers gradually achieved nanoscaling of PersL materials. In 2007, Chermont et al. [5] first applied PLNPs to bioimaging, confirming that they can completely avoid in-situ excitation and thus largely avoid tissue autofluorescence interference, ushering in a new era of PLNPs in biomedical applications. Compared with organic PersL systems, inorganic PLNPs (InPLNPs) offer unique advantages such as high luminous brightness, long afterglow life, high chemical stability, wide adjustable emission wavelength range (from visible to near-infrared two-zone), strong resistance to photobleaching, and internal recharging capability [8,9]. After nearly two decades of development, InPLNPs have expanded from early aluminate systems to a diverse array of host matrices including gallates, silicates, fluorides and titanates [1]. Their emission bands have gradually shifted from visible region to the first near-infrared (NIR-I) and even the second near-infrared (NIR-II) window, with continuous improvements in tissue penetration depth and anti-interference capabilities [8]. Accordingly, InPLNPs have made significant progress in fields including bioimaging, biosensing, and disease treatment [10,11]. Notably, recent years have witnessed a surge of innovative research focusing on their sensing applications. Researchers have developed multiple sensing construction strategies, including persistent luminescence resonance energy transfer (PLRET) [12], ratiometric self-calibration [13], target-activated sensing [14], sensor arrays [15], and lateral flow assay strips [16]. These enable highly sensitive detection of targets such as antibiotics, pesticide residues, heavy metal ions, nucleic acids, and proteins, advancing InPLNP-based sensing from basic research toward practical application scenarios [17,18], including clinical in vitro diagnosis and on-site environmental detection.

This review focuses on InPLNP systems. Starting with material classification and luminescence mechanisms, it systematically summarizes the current mainstream sensing construction strategies and application advances, analyzes the application advantages and existing limitations of various technical routes, and discusses the core challenges and future development in this field, aiming to provide references for the design and translational application of novel persistent luminescence sensing probes. Several closely related reviews on persistent luminescence nanomaterials have been published in recent years. For instance, Zhao et al. summarized stimuli-responsive PLNP-based sensors [17], Zhao et al. reviewed spinel-type PLNPs from mechanisms to applications [18], Chan and Chang discussed NIR persistent luminescent nanoparticles in cancer analysis [19], and Luo et al. focused on surface-modified persistent luminescence probes for biosensing and bioimaging [20]. However, these prior reviews either concentrate on specific material families or broadly cover bioimaging and theranostics alongside sensing. In contrast, the present review is exclusively dedicated to InPLNPs for sensing and detection applications, providing a focused and systematic account of material design, sensing strategies, and analytical performance. Importantly, this review places particular emphasis on the most recent five years of research progress, capturing emerging developments such as ratiometric aptasensors, nanozyme-coupled systems, and multiplexed POCT platforms that have rarely been comprehensively covered in earlier reviews. By focusing on these latest advances, we aim to provide a timely and up-to-date reference for researchers entering this rapidly evolving field.

2. Overview of InPLNPs

2.1. Main Matrix Systems

InPLNPs encompass a wide variety of types, and their luminescence properties are highly dependent on the matrix lattice and dopant ions. As listed in Table 1, different matrix systems differ significantly in emission wavelength, PersL duration, and chemical stability, making them suitable for distinct sensing application scenarios correspondingly.

Aluminate is the earliest extensively studied PersL material system. A typical representative is $SrAl_2O_4:Eu^{2+}$, Dy^{3+}, which features high brightness, long afterglow duration (over 10 h at room temperature), mature fabrication processes and low cost. However, its poor chemical stability and susceptibility to hydrolysis restrict direct applications in biomedicine and sensing [21,22]. In addition, aluminate systems mainly emit green visible light (~520 nm) with limited tissue penetration, which is unfavorable for sensing in complex biological fluids and *in vivo* scenarios. Silicate systems (e.g., $Sr_2MgSi_2O_7:Eu^{2+}$, Dy^{3+}) exhibit better chemical stability and water resistance, with an afterglow duration exceeding 10 h, making them promising candidates for biomedical applications [23]. Nevertheless, its emission wavelength still falls mainly in the visible light region, and the synthesis temperature is relatively high (>1200 °C), making agglomeration easily occurring during nanoscaling, limiting its application in complex matrix sensing [19].

Gallate systems are currently the most widely used NIR PersL materials for sensing applications. Among them, Cr^{3+}-doped $ZnGa_2O_4$ ($ZnGa_2O_4:Cr^{3+}$, ZGO:Cr^{3+}) is one of the most representative materials. It emits intense NIR afterglow at approximately 700 nm, with favorable tissue penetration, good biocompatibility, high chemical stability and relatively mild synthesis conditions [24,25]. From the perspective of sensing applications, ZGO is one of the

best-performing PLNP host matrices to date, yet its quantum yield (usually <10%) still leaves much room for improvement [26]. Studies have shown that Sn^{4+} co-doping can introduce deeper antisite defect traps, extending the afterglow duration from hours to tens of hours while significantly enhancing luminescence intensity [27].

The zinc gallogermanate (ZGGO) system is an emerging PersL host matrix in recent years. By introducing Ge^{4+} to partially replace Ga^{3+} in ZGO, it modulates lattice defect concentration and trap structure to optimize PersL performance [28]. Through further defect engineering, the ZGGO system has achieved controllable synthesis of monodisperse sub-10 nm nanoparticles with greatly improved PersL performance, combining small size and bright PersL to suit intracellular sensing and *in vivo* tracking scenarios [29]. Despite its tunable PersL performance, the ZGGO system still needs improvement in synthesis reproducibility and batch-to-batch consistency.

2.2. Nanoscaling Synthesis Strategies

The synthesis method of InPLNPs has a significant impact on their microstructure, particle size distribution, and luminescence performance. Currently, common methods for preparing InPLNPs include high-temperature solid-phase method, hydrothermal/solvothermal method, template method, sol-gel method, and high-temperature thermal decomposition method. A comparative summary of these methods is provided in Table 2.

The high-temperature solid-phase method is the traditional method for preparing long afterglow materials, synthesizing bulk materials through high-temperature solid-phase reactions, which are then mechanically ground to obtain nanoparticles. As a "top-down" preparation method, it is simple to operate and low in cost, but the resulting InPLNPs have uneven particle sizes, poor dispersion, and many surface defects, which is unfavorable for building high-performance sensing platforms. Paterson et al. [30] ground $SrAl_2O_4:Eu^{2+}$, Dy^{3+} bulk materials to the nanometer scale using the ball milling method, and used them as PersL report probes for lateral chromatography test strips. Although this method achieved proof of concept, the afterglow brightness of InPLNPs significantly decreased after grinding, and the wide particle size distribution limited further improvement in detection sensitivity.

In comparison, bottom-up synthesis methods enable better control over the size, morphology and surface properties of InPLNPs. The sol–gel method is one of the key approaches for synthesizing PersL materials. Its main procedure involves first hydrolyzing metal salt precursors into a sol, followed by the addition of ligands and crosslinking agents to form a gel, and finally subjecting the product to high-temperature calcination [28]. InPLNPs prepared via this method exhibit nanoscale dimensions and excellent afterglow performance. Moreover, their optical properties, particle size and morphology can be modulated by adjusting synthesis conditions, such as raw material composition, calcination temperature and ligands.

The hydrothermal/solvothermal method is a synthetic approach in which precursors are mixed in an appropriate solvent and then subjected to a heating reaction in a sealed high-pressure environment. Wang et al. [29] reported the preparation of sub-10 nm $ZGGO:Cr^{3+}$ via hydrothermal reaction. The product exhibited enhanced *in vivo* rechargeable NIR PersL imaging performance, displaying great potential for autofluorescence-free targeted bioimaging. Wei et al. [24] reported a solvothermal synthetic route for preparing $ZGGO:Cr^{3+}$ nanoparticles with particle size tunable from 4 to 31 nm and afterglow duration longer than 20 h. Compared with other synthetic methods, the hydrothermal/solvothermal method features relatively mild reaction conditions and yields InPLNPs with better dispersity. By adjusting parameters such as pH and precursor concentration, the size, morphology and luminescence properties of InPLNPs can be tuned, expanding the research scope of persistent luminescence materials in biomedicine [29]. However, in general, products obtained via this method show relatively weak afterglow performance, and high-temperature calcination is often combined to improve their optical properties.

In recent years, researchers have been committed to developing size- and morphology-controllable synthesis strategies to improve the performance reproducibility of InPLNPs and the efficiency of surface functionalization. The template method is currently an important strategy for preparing InPLNPs with specific morphologies. This method typically uses mesoporous silica as a template, deposits precursor ions on the template surface or within its pores, and then obtains size- and morphology-controllable InPLNPs via annealing [31]. Owing to their regular morphology and uniform dispersion, InPLNPs prepared by this method have been widely used in optical sensing and research on nanocarriers for imaging-guided drug delivery.

In addition, the high-temperature thermal decomposition method prepares InPLNPs via the thermal decomposition of metal salt precursors in high-boiling solvents [32]. It enables the regulation of particle size and PersL performance by varying solvents, reaction temperatures and dopant ions, and is one of the optimal approaches for synthesizing ultrasmall, monodisperse InPLNPs. Wei et al. [33] fabricated uniform and monodisperse core-shell $NaYF_4:Tb@NaYF_4:Eu$ nanoparticles by thermal decomposition, achieving X-ray-activated Eu^{3+} PersL via interfacial energy transfer, with high light yield for flexible X-ray imaging.

Table 1. Summary of representative InPLNP matrix systems and their properties.

Matrix	Representative Composition	Activator	Emission (nm)	Excitation Source	Duration	Advantages	Limitations
Aluminate	$SrAl_2O_4:Eu^{2+}$, Dy^{3+}	Eu^{2+}	~520 (green)	UV	>10 h	High brightness, low cost	Poor water stability, visible emission only
Silicate	$Sr_2MgSi_2O_7:Eu^{2+}$, Dy^{3+}	Eu^{2+}	~470–520 (green)	UV	>10 h	Better water stability	High synthesis temperature, agglomeration, visible emission only
Gallate	$ZnGa_2O_4:Cr^{3+}$	Cr^{3+}	~700 (NIR-I)	UV/Vis/X-ray	Hours to tens of hours	Good stability, NIR emission, biocompatibility, mild synthesis	Moderate quantum yield (<10%)
Gallogermanate	ZGGO:Cr^{3+}	Cr^{3+}	~700 (NIR-I)	UV/Vis/X-ray	Tens of hours	Tunable traps, small size	Batch-to-batch variability
Fluoride	$NaYF_4:Ln^{3+}$	Ln^{3+}	Visible-NIR	X-ray/UV	Minutes to hours	Sharp emission lines	Short afterglow

Table 2. Comparison of nanoscaling synthesis strategies for InPLNPs.

Method	Size Controllability	Dispersibility	Crystallinity	Afterglow Intensity	Scalability	Key Limitations
Solid-phase (ball milling)	Poor	Poor	High	High for bulk (reduced after grinding)	High	Uneven size, surface defects, grinding required
Sol-gel	Moderate	Moderate	Moderate-high	High	Good	High calcination temperature, agglomeration risk
Hydrothermal/solvothermal	Good	Good	Moderate	Moderate-low	Moderate	Weak afterglow, often needs post-calcination
Template	Good	Good	Moderate-high	Good	Low	Complex procedure, limited yield
Thermal decomposition	High	High	High	Moderate-high	Low	Complex operation, high cost

At present, the synthesis of InPLNPs still faces several key challenges. The primary issue is the balance between particle size and luminescence performance: reducing particle size usually leads to increased surface defects and decreased luminescence efficiency. How to achieve the controllable synthesis of sub-10 nm InPLNPs while maintaining high luminescence efficiency remains an urgent issue to be addressed.

2.3. Surface Functionalization Strategy

Compared to bulk phase materials, nanoscale InPLNPs have a higher specific surface area. Their surface dangling bonds and defects form abundant shallow traps that can not only accelerate nonradiative charge carrier recombination and reduce PersL efficiency but also serve as surface-responsive sites for sensing. This is one of the core features distinguishing nanoscale and bulk PersL materials. Modulating the surface trap states of PLNPs via surface modification can optimize afterglow performance and enhance colloidal stability while introducing specific recognition sites, making it a pivotal step in contemporary sensing probe design.

Silica (SiO_2) coating is a versatile strategy for enhancing the aqueous stability of PersL nanomaterials, generally falling into two categories: dense SiO_2 shells and mesoporous SiO_2 ($mSiO_2$) shells. Dense SiO_2 shells fully encapsulate InPLNP cores to isolate them from external erosion, effectively addressing the poor aqueous stability of hydrolysis-prone materials such as aluminates. Meanwhile, they passivate surface defects, reduce nonradiative recombination, and improve PersL intensity. Zou et al. [34] developed a silica shell-assisted synthesis strategy to fabricate monodisperse ZGO:Cr^{3+}@SiO_2 core-shell nanoparticles. Beyond protecting InPLNP cores, $mSiO_2$ coating provides ordered pore architectures and a large specific surface area, endowing InPLNPs with both functionalization feasibility and cargo loading capacity. It is a prevalent approach for constructing responsive sensing probes and lays a material foundation for integrated theranostic platforms [35,36].

Polymer modification forms a polymeric coating on the material surface via physical adsorption or covalent grafting. It effectively improves the colloidal stability and biocompatibility of InPLNPs, and introduces stimuli-responsive properties toward pH, redox, temperature and other triggers to accommodate the sensing demands of complex microenvironments. Liu et al. [37] systematically investigated the effects of hydrophilic polymer coatings (e.g., PEG, polydopamine) on InPLNPs in *in vivo* imaging, and confirmed that polymer coatings could significantly enhance the colloidal stability and biocompatibility of InPLNPs. For sensing applications, polymer coatings can also reduce nonspecific adsorption and improve detection specificity. The universal optode-based PLNP nanosensor platform proposed by Sodia et al. [38] provided a new paradigm for surface functionalization. By embedding PLNPs in a polymer matrix, complex surface chemical modification was circumvented while preserving sensing performance. This strategy is expected to simplify the fabrication workflow of PLNP sensors and improve batch-to-batch reproducibility.

To endow InPLNPs with target-specific recognition ability, biorecognition molecules including antibodies, aptamers, peptides and enzymes are conjugated onto their surface. This is a critical step for enabling specific InPLNP-based sensing. Aptamers are the most widely used recognition molecules in InPLNP sensing, thanks to their high affinity, high specificity, and ease of synthesis and modification. For instance, Zhao et al. [39] conjugated carbendazim aptamers onto PLNPs to construct a ratiometric aptasensor for carbendazim detection.

It should be noted that surface modification, while improving the colloidal stability and specificity, can also affect the persistent luminescence properties of InPLNPs in both positive and negative ways. Coating layers such as SiO_2 and polymers may influence surface trap states, charge transfer dynamics, and quenching pathways. For example, dense SiO_2 shells can passivate surface defects and reduce nonradiative recombination, thereby enhancing PersL intensity. However, thick polymer coatings may increase hydrodynamic size and create new surface trap states, potentially reducing the detectable PersL signal. Similarly, the conjugation of biorecognition molecules improves targeting specificity but may also alter the surface charge, colloidal stability, and accessibility of surface traps. Both the positive and the negative effects of surface modification should therefore be carefully evaluated during probe design. Besides, surface modification often adds synthetic steps and amplifies batch-to-batch variability. Improving preparation reproducibility and standardization without compromising modification performance is a key challenge for translating InPLNP sensing probes into practical applications.

2.4. PersL Mechanisms and Performance Regulation

2.4.1. PersL Mechanisms

The PersL of InPLNPs follows the carrier trapping–release model, centered on the trapping and thermal release of charge carriers by lattice trap energy levels. As illustrated in Figure 1, when excited by external stimuli such as ultraviolet light, visible light or X-rays, valence electrons in the host matrix or activator ions are promoted to the conduction band, forming charge carriers (free electrons and holes). A fraction of these carriers are captured

and stored by trap levels generated by lattice defects and dopant ions. After excitation ceases, thermal perturbation at room temperature drives the slow release of trapped carriers back to the conduction/valence band. They eventually return to the excited state of activator ions and undergo radiative transition, producing persistent luminescence [9,40].

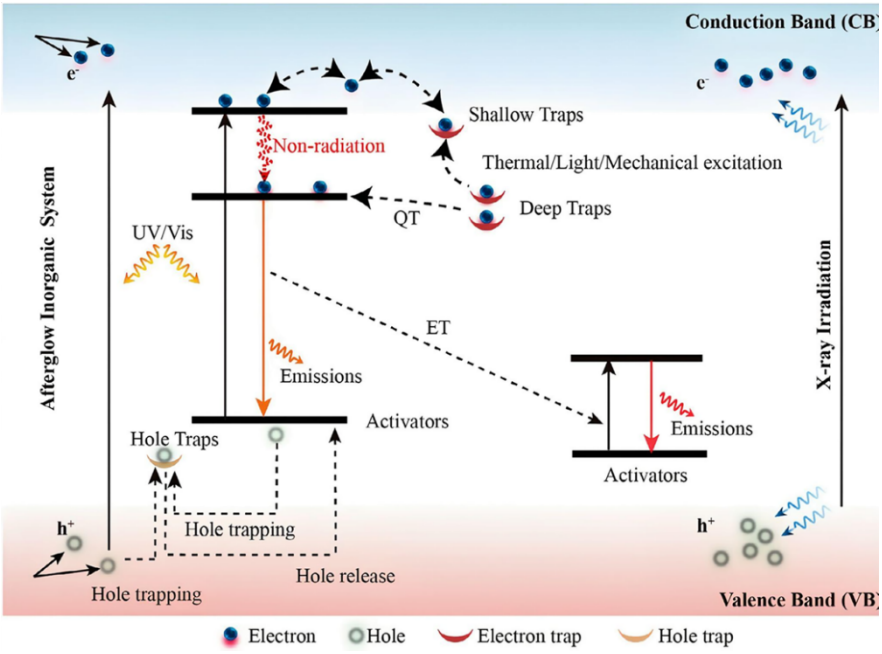


Figure 1. Schematic diagram of the afterglow luminescence mechanism in inorganic systems. Reproduced with permission from ref. [9]. Copyright 2025, Wiley.

The luminescence performance of InPLNPs is synergistically governed by the matrix lattice, dopant ions and defect structures. The host matrix provides the structural framework and trap environment. Dopant ions (activators), including rare-earth species (e.g., Ce^{3+}, Eu^{2+}, Eu^{3+}) and transition metal species (e.g., Cr^{3+}, Mn^{2+}, Mn^{4+}), serve as luminescent centers to modulate emission wavelength [41], while co-dopant ions (co-activators, e.g., Sn^{4+}) are used to introduce or tune trap energy levels [27]. Trap depth and concentration are critical parameters determining PersL intensity and duration [42], as depicted in Figure 2. Specifically, trap concentration defines the overall carrier trapping capacity, whereas trap depth dominates the release kinetics of trapped charge carriers [43]. Appropriate trap depths enable PersL lasting from hours to tens of hours at room temperature [44]. Excessively shallow traps cause rapid carrier release and short PersL, whereas overly deep traps impede carrier release at room temperature and fail to generate effective afterglow [45].

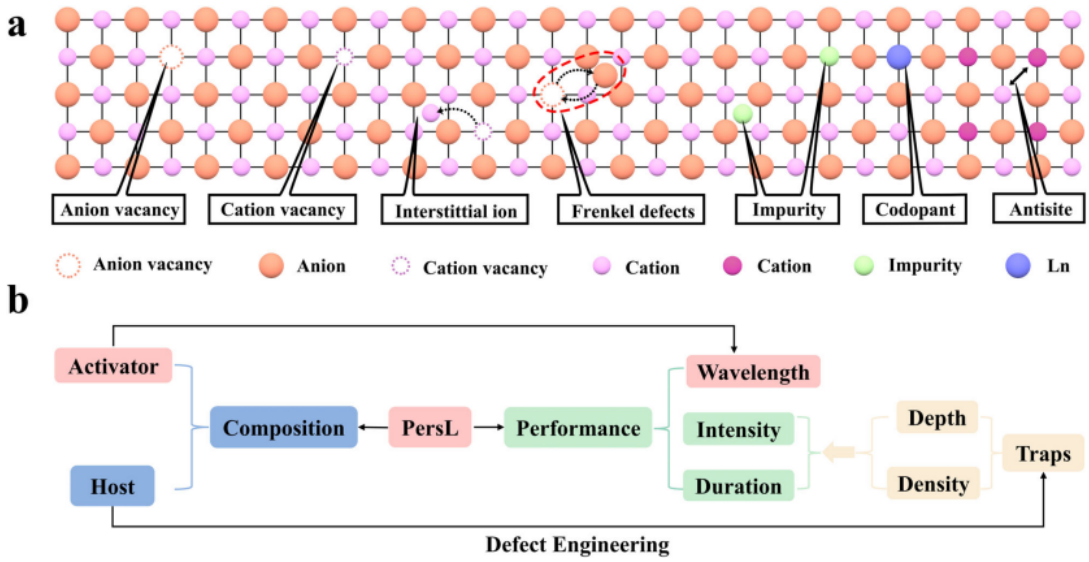


Figure 2. (**a**) Common point defects within the crystal lattice of PersL materials; (**b**) Relationship among composition, performance, and traps in PersL materials. Reprinted with permission from ref. [42] Copyright 2025, Wiley.

2.4.2. PersL Regulation Strategy

The PersL performance of InPLNPs, including afterglow intensity, duration, emission wavelength, and recharge efficiency, directly determines their detection sensitivity and reliability in sensing applications. Various regulatory strategies have been developed for targeted optimization of InPLNPs performance to accommodate diverse biosensing scenarios [46].

Among these strategies, ion co-doping stands as one of the most efficient and versatile core modulation approaches. The introduction of aliovalent or rare-earth ions induces lattice distortion, enabling precise tuning of trap depth and concentration, thereby markedly prolonging PersL lifetime and enhancing luminescence efficiency [47,48]. Co-doping with dual activators enables multi-band synergistic emission for the construction of ratiometric sensing probes, which effectively eliminates interferences from concentration fluctuations and luminescence attenuation, finally improving the accuracy of quantitative detection.

Host defect engineering represents a fundamental route to regulating PersL performance. By controlling synthesis conditions (temperature, atmosphere, precursor ratio, etc.) and post-treatment processes (annealing, reduction/oxidation treatment, etc.), the type and concentration of defects (e.g., oxygen vacancies, antisite defects) can be modulated, which in turn shapes PersL performance [40]. This approach enables effective tuning of PersL intensity and decay kinetics without extrinsic doping. Nevertheless, defect concentration is difficult to quantify precisely, and batch-to-batch stability is relatively poor. Thus, it is usually deployed synergistically with co-doping strategies.

Tuning of nanoscale size and morphology can modify surface defect density and charge carrier transport behavior, optimizing luminescence properties and biocompatibility [24]. Interface modification and core-shell structural design can passivate surface defects, suppress luminescence quenching, improve water dispersibility and sensing response of PersL, and are important post-treatment methods to enhance the practical performance of PersL [20].

Notably, modulating excitation and charging modalities can overcome the constraints of application scenarios. Conventional ultraviolet light is only applicable to in vitro detection, while X-rays and NIR light enable non-invasive deep-tissue charging to support long-term dynamic *in vivo* monitoring. Different excitation sources can precisely match materials featuring different levels of trap energies [49]. Recently, research on new excitation methods has also made significant progress. Two works reported electrical modulation of inorganic PersL. A direct current electric field enhanced the initial PersL brightness of $SrAl_2O_4:Eu^{2+}$, Dy^{3+} by accelerating shallow-trap electron release via the conduction band [50]. Another alternating current-driven ZnS-based electroluminescent device realized electrically chargeable PersL with ~0.3 eV traps, enabling energy storage and time-temperature indicator applications [51].

2.4.3. Key Definitions and Measurement Conditions

Quantitative comparison of InPLNPs requires that related kinetic and acquisition terms be used unambiguously, because several quantities are routinely quoted but often confused, and they must not be used interchangeably. The luminescence lifetime (τ) and its inverse, the decay constant ($k = 1/\tau$), characterize the intrinsic first-order trap-release kinetics. The afterglow duration is instead a practical quantity set by the detection threshold, namely how long the emission remains above the limit of the eye or of an instrument, rather than τ alone. The delay time and integration time are acquisition settings rather than material properties. The delay selects which portion of the decay curve is sampled and rejects short-lived background fluorescence, while the integration gate trades signal gain against background and decay fidelity.

It is also important to recognize that measured PersL intensity is not an intrinsic material constant. For a given material, the reported brightness varies with the excitation wavelength and irradiance, charging duration, delay time, integration window, temperature, particle concentration, detector response, and charging history, including prior irradiation that fills or empties the traps. Given the marked differences in these conditions among laboratories, direct comparison of reported intensity and decay values between studies is not feasible. To enable meaningful cross-study comparisons, a standardized reporting framework with well-defined charging and readout protocols is therefore necessary.

3. Sensing Principles and Strategies

In terms of sensing principles, all PersL detection systems achieve quantitative transduction of target concentrations via target-induced direct or indirect modulation of PersL parameters, including intensity, lifetime and emission wavelength. Based on distinct target response mechanisms, researchers have developed a range of well-established sensing design strategies, advancing PersL sensing toward high sensitivity, high specificity and accurate quantification.

3.1. Detection Based on InPLNP Capture and Enrichment

This strategy uses InPLNPs as signal tags and capture target analytes through specific recognition units such as aptamers and antibodies. Since the PersL signals of InPLNPs can be collected after excitation stops, the detection process is free from excitation interference, making them especially suitable for low-concentration detection where long-term signal accumulation is required. The combination of magnetic nanoparticles and InPLNPs represents a classic example of this strategy. For example, Fe_3O_4 nanoparticles serve as capture and separation units while InPLNPs act as signal units, enabling target enrichment and low-background detection via magnetic separation [52].

3.2. PLRET-Based Sensing

Persistent luminescence resonance energy transfer (PLRET) is one of the most widely adopted sensing strategies. In this approach, InPLNPs serve as energy donors. In the presence of the target, the energy transfer efficiency is modulated by altering the distance or the spectral overlap between donors and acceptors, leading to detectable changes in the PersL signal. The long-lived luminescence property of InPLNPs endows them with unique advantages in time-resolved PLRET detection. By collecting signals through time-gated control, short-lived background fluorescence and scattered light can be effectively filtered out, enabling ultrasensitivity detection [53].

Commonly used acceptors for PLRET include fluorescent dyes, quantum dots, and gold nanoparticles. Efficient energy transfer can be achieved by tuning the spectral overlap and spatial distance between the donor and acceptor. In a typical PLRET sensing system, the PerL of InPLNPs is quenched by the acceptors via resonance energy transfer. Upon the introduction of the target analyte, competitive binding or conformational changes trigger the release of the acceptors from the InPLNP surface, leading to the recovery of the PerL signal. This "turn-on" design effectively avoids false-positive signals and substantially improves the detection accuracy [54].

3.3. Ratiometric Sensing Strategy

Ratiometric detection achieves quantitative analysis by measuring the PersL signal ratio of two different emission wavelengths. This approach enables self-calibration, effectively eliminates external interference, and improves detection accuracy and reliability.

Dual-emission InPLNPs are a crucial foundation for building ratiometric sensors. A single-particle dual-emissive InPLNPs ratiometric probe can be constructed using dual characteristic emission peaks of a single activator ion or by employing a co-doping strategy with two luminescent centers [15]. For example, the $NaYF_4$@$NaYF_4$ core-shell PersL nanostructure based on Er^{3+} doping has double emission peaks at 528 nm and 545 nm, originating from $^2H_{11/2}\rightarrow{}^4I_{11/2}$ and $^4S_{3/2}\rightarrow{}^4I_{15/2}$ transitions, respectively. By designing temperature-dependent changes in intensity ratio, self-calibrated ratiometric temperature sensing can be achieved [55]. Furthermore, an additional luminescent probe can be introduced to construct a donor–acceptor pair with PLNPs. By exploiting the target concentration-dependent FRET efficiency, precise ratiometric quantification can be realized via the dual-channel signal ratio [39].

3.4. Nanozyme-PersL Coupling-Based Sensing

In recent years, the combined strategy of nanozymes and InPLNPs has attracted widespread attention. MnO_2 nanozymes can effectively quench the PersL of InPLNPs, while target analytes (such as glutathione) can restore PersL signals by reducing MnO_2 or regulating its enzymatic activity [56,57]. The advantages of this strategy are [58]: (1) MnO_2 nanozymes serve as both quenching agents and recognition units, simplifying sensor design; (2) The catalytic reaction of nanozymes can amplify detection signals and improve sensitivity; (3) On-site testing can be achieved through simple platforms such as paper chips.

To facilitate direct comparison among these strategies, Table 3 summarizes their key characteristics in terms of signal mechanism, sensitivity, anti-interference capability, complexity, limitations, and applicable targets.

Table 3. Comparison of representative InPLNP-based sensing strategies.

Strategy	Signal Mechanism	Sensitivity	Anti-Interference	Complexity	Key Limitations	Applicable Targets
Capture and enrichment	Target capture by recognition units	High	High	Low-moderate	Nonspecific adsorption	Nucleic acids, proteins, pathogens
PLRET	Energy transfer between donor and acceptor	Very high	High	Moderate	Distance- and spectral overlap- dependent	Small molecules, nucleic acids
Ratiometric	Dual-wavelength signal ratio	Moderate-high	Very high	High	Complex design of dual-emission probes	Ions, small molecules, temperature
Nanozyme-coupled	Catalytic quenching/restoration	Very high	Moderate	High	Nanozyme stability, potential interference	ROS, GSH, H_2O_2

4. InPLNP-Based Sensing Applications

With their unique advantage of a greatly suppressed autofluorescence background, InPLNPs-based sensing applications have widely covered various targets such as biological macromolecules, reactive oxygen species, metal ions, and physiological parameters, demonstrating significant value in food safety, environmental monitoring, clinical diagnostics, and other fields.

4.1. Food Safety and Environmental Pollution Testing

Highly sensitive detection of trace pollutants in complex food substrates and environmental systems is a core requirement in public health and ecological monitoring. With features such as a minimal autofluorescence background, strong resistance to matrix interference, and high detection sensitivity, InPLNPs demonstrate significant advantages in both food safety and environmental pollution fields, enabling precise quantification and rapid screening of trace hazards in complex systems [59,60]. Mycotoxin contamination in agricultural products poses a serious threat to human and animal health, so the development of sensors for sensitive quantification of mycotoxins in food matrices is essential for food safety surveillance. By leveraging the unique properties of PLNPs, including no requirement for in situ excitation and near-zero autofluorescence interference, coupled with ratiometric and/or PLRET signal transduction mechanisms, a variety of InPLNP-based aptasensors have been developed for the detection of multiple mycotoxins in food matrices, including ochratoxin A (OTA) [61,62], aflatoxin B1 (AFB1) [63,64], and zearalenone (ZEN) [64].

Pesticide residue testing is an important area of food safety and environmental monitoring. Carbendazim (CBZ) is a broad-spectrum benzimidazole fungicide. Excessive CBZ can accumulate in agricultural products and the environment, and undergo biomagnification through the food chain, thereby posing a potential threat to human health and ecosystems. Recently, Zhao et al. [39] reported a complementary DNA (cDNA)-free ratiometric aptasensor based on InPLNPs for ultrasensitive detection of CBZ (Figure 3A). Instead of conventional quencher-labeled cDNA, the sensor innovatively introduced methylene blue (MB) as a multifunctional substitute acting as both the energy acceptor and the second signal channel. During detection, MB quenched the PersL of InPLNPs at 542 nm and produced its own emission at 700 nm. Upon CBZ addition, the aptamer bound to the target and released MB, turning on the 542 nm signal and turning off the 700 nm signal for interference-resistant dual-channel ratiometric detection. The sensor achieved a detection limit of 0.682 ng/mL and was successfully applied to CBZ detection in multiple real food samples including cherry tomatoes, oranges and lettuce.

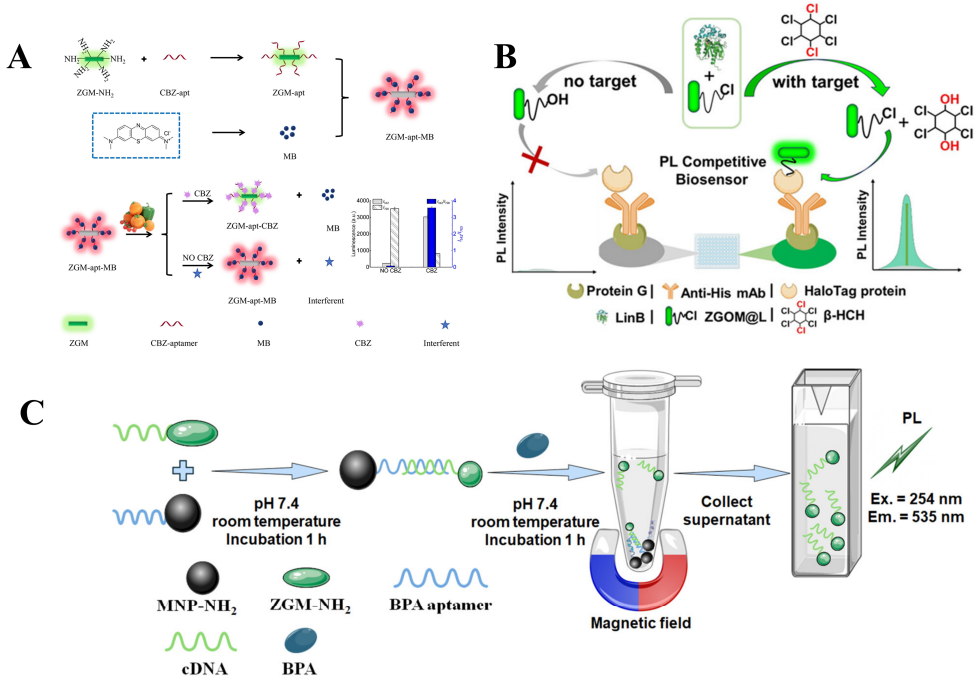


Figure 3. (**A**) Design and principle of ZGM-apt-MB ratiometric aptasensor for ultrasensitive and selective detection of CBZ. Reprinted with permission from ref. [39]. Copyright 2026, American Chemical Society. (**B**) Schematic illustration of the oersistent luminescence competitive enzyme biosensor for β-HCH detection. Reprinted with permission from ref. [65]. Copyright 2026, American Chemical Society. (**C**) Design of the MNP-apt@ZGM-cDNA aptasensor for sensing BPA. Reprinted with permission from ref. [66]. Copyright 2025, American Chemical Society.

β-Hexachlorocyclohexane (β-HCH) is the most toxic and environmentally persistent organochlorine pesticide residue. It readily accumulates in adipose tissue and resists metabolic degradation, rendering its highly sensitive detection vital for accurately evaluating food safety and human health risks. Recently, a competitive enzyme biosensor based on InPLNPs was reported for the ultrasensitive detection of β-HCH (Figure 3B) [65]. In this work, HaloTag ligand-modified InPLNPs served as both optical reporters and competitive substrates for dehalogenase LinB. β-HCH preferentially depleted the catalytic activity of LinB, allowing InPLNPs to covalently bind to immobilized HaloTag proteins. The luminescence signal intensified with rising β-HCH concentration, achieving a detection limit of 0.02 ng/mL. The sensor was successfully applied to autofluorescence-free detection of trace β-HCH in vegetable samples.

Bisphenol A (BPA) is a typical endocrine-disrupting chemical that can migrate from food packaging materials into food, posing significant health risks. Recently, Yan Group has developed various InPLNP-based aptasensors for BPA monitoring in seafood and food packaging materials [54,66]. For example, BPA aptamer-functionalized Fe_3O_4 nanoparticles served as both the recognition/separation unit and the PersL quenching unit, while cDNA-modified $Zn_2GeO_4:Mn^{2+}$ InPLNPs acted as the signal source. The two components formed a PersL-quenched complex via aptamer-cDNA hybridization. In the presence of BPA, the target competitively bound to the aptamers and released InPLNPs, generating a PersL signal proportional to BPA concentration (Figure 3C). This sensor revealed that photoaging and heating significantly increased the release of BPA from packaging materials into water, posing a toxic risk to human health [66].

Overall, InPLNPs sensing technology has greatly simplified the pretreatment process for food and environmental samples, significantly improving detection efficiency and sensitivity. However, several limitations remain to be addressed, including limited throughput for simultaneous multi-component detection and suboptimal applicability in complex field scenarios. Future development of multi-wavelength encoding and portable detection equipment will further promote the practical application of this strategy in on-site rapid testing.

4.2. Biomarker and Immune Checkpoint Detection

Biological macromolecules (nucleic acids, proteins, enzymes, etc.) are core markers for early disease diagnosis, and their trace precision detection has long been a key focus in analytical chemistry. PersL sensing can eliminate background fluorescence interference from complex matrices such as serum and cell lysate, offering significant advantages in low-abundance biomarker detection.

In nucleic acid sensing, Wang et al. used $Zn_2GeO_4:Mn^{2+}$ PLNPs as donors for the first time to construct time-resolved PLRET molecular beacon probes for microRNA21 detection [12]. In the absence of the target, BHQ3 remained in close proximity to the PLNPs and quenched luminescence via PLRET. Upon binding to microRNA21, the beacon unfolded and BHQ3 moved apart, leading to the recovery of PersL. This probe exhibited a linear range of 0.1–10 nM, with detection limits 1–2 orders of magnitude superior to that of traditional molecular beacons. It has been successfully used for autofluorescence-free detection of microRNA21 in serum and cell lysates.

Immunosensing is one of the most well-established application fields of PersL materials. Zhao's group [67] constructed a PLRET-based aptasensor for the detection of prostate-specific antigen (PSA) using ZnGeO:Mo PersL nanorods as probes and Au@Ag@SiO_2 nanoparticles as quenchers, achieving a limit of detection of 9.2 pg/mL. Clinical diagnosis typically requires simultaneous detection of multiple tumor markers to improve diagnostic accuracy. Concurrently, Zhao's group reported an autofluorescence-free aptasensor for dual tumor markers [68]. Through ion doping, green-emitting Zn_2GeO_4:Mn nanorods (ZGO:Mn) and near-infrared-emitting $ZnGa_2O_4$:Cr nanoparticles (ZGC) were fabricated. With non-overlapping emission colors and slow decay kinetics, the two materials served as dual-channel detection probes for PSA and carcinoembryonic antigen (CEA). Based on aptamer recognition-blocked PLRET quenching (Figure 4A,B), the targets induced recovery of the dual-color PersL signals, enabling sensitive detection of PSA and CEA with limits of detection as low as 8.9 fg/mL (PSA) and 72 fg/mL (CEA), respectively. The sensor was successfully applied to monitor PSA and CEA levels in real serum samples. This study opens a new avenue for the application of multicolor PLNPs with tailored decay patterns in the field of time-resolved fluoroimmunoassay.

PD-L1 expression level is a key predictive biomarker for the efficacy of immune checkpoint blockade therapy (ICBT). Accurately evaluating PD-L1 helps stratify eligible patients, develop individualized treatment regimens and avoid ineffective therapy. In the latest study, Wang et al. reported a NIR PersL nanoprobe for highly sensitive imaging of PD-L1 immune checkpoints in microtumors during immunotherapy [69]. Monodisperse NIR PLNPs with a size of ~52 nm were synthesized via a mSiO_2-assisted approach, then surface-functionalized with PEG and conjugated with anti-PD-L1 antibodies to construct the targeted probe mZ-PD-L1. This probe effectively distinguished PD-L1 expression levels across different tumor cell lines, and enabled highly sensitive, high SNR and precise imaging of PD-L1 in sub-1 mm microtumors and lymph node micrometastases in mouse models, providing a novel tool for early evaluation of immunotherapy efficacy.

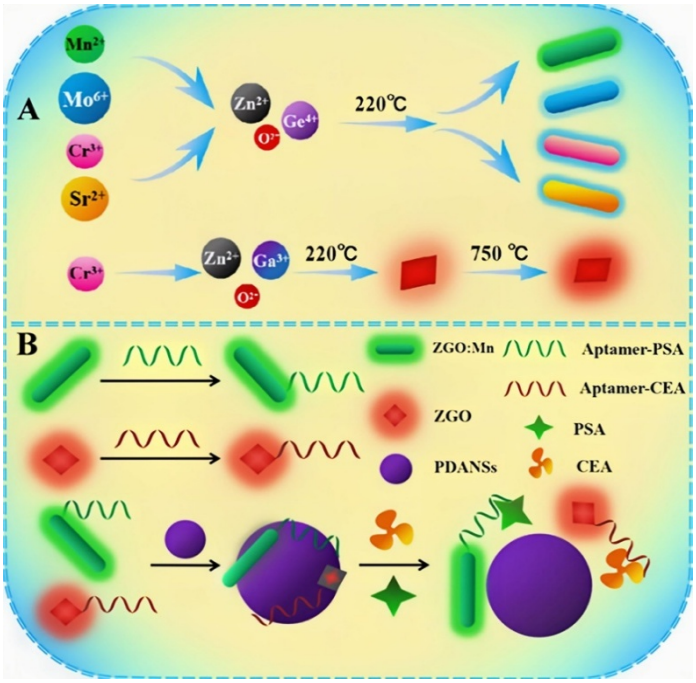


Figure 4. Schematic illustration of (**A**) the controllable preparation of ZGO NRs and ZGC PLNPs by doping different elements, and (**B**) autoluminescence-free dual detection of PSA and CEA through ZGO:Mn NRs and ZGC NPs. Reprinted with permission from ref. [68]. Copyright 2020, American Chemical Society.

4.3. Detection of Pathogenic Microorganisms and Bacteria

Rapid detection of pathogenic microorganisms is of great significance for clinical diagnosis and public health safety. Feng et al. proposed a multiplex SARS-CoV-2 detection strategy based on a PersL lifetime/color binary encoding strategy [70]. Ion-doped/co-doped $CdSiO_3$ nanoparticles with tunable PersL lifetime and emission properties were successfully fabricated via a PLRET approach, enabling a new temporal coding dimension within a seconds-to-minutes range in three individual color channels, with each channel capable of decoding at least four barcodes. The functionalized PersL nanoplatform achieved simultaneous quantitative detection of five SARS-CoV-2 biomarkers (IgG, IgM, ORF1ab, RdRp and E) with sub-nanomolar limits of detection, providing a novel tool for high-throughput optical multiplex detection.

Chen et al. reported a PLNPs-based autofluorescent-free molecular imprint aptasensor (MIP-aptasensor) for detecting H5N1 virus [71]. The sensor comprised magnetic molecularly imprinted polymers (MIP) and aptamer-functionalized $Zn_2GeO_4:Mn^{2+}$ PersL nanorods (ZGO-H5N1 Apt). Following dual recognition of the H5N1 virus via both MIP and aptamers, a PersL signal was generated (Figure 5A). The sensor exhibited a limit of detection of 0.0128 HAU/mL (1.16 fM) and an imprinting factor of 6.72. It effectively eliminated autofluorescence interference from serum samples, achieving highly sensitive and selective detection of H5N1 in complex biological matrices.

Additionally, PLNPs sensing can be used for bacterial activity assessment and antibiotic sensitivity detection. Wang's group has reported a series of advances in this area [72–75]. Microbial communication monitoring is essential for understanding gut microbiota and biomanufacturing. They reported a surface-confined PersL strategy using core-shell ZGGO@ZGGO:Cr PLNPs with amplified FRET for azoreductase (AzoR) detection [72]. The probe exhibited 1.6-fold higher PLRET efficiency between PLNPs and surface-bound azo black hole quencher (BHQ-3). The bacterial extracellular AzoR specifically cleaved azo bonds in BHQ-3 and recovered the PersL in a dose-dependent manner, with AzoR secretion reaching peak during the exponential growth phase. In co-culture, R. palustris and S. putrefaciens showed enhanced AzoR and lycopene production, with positive correlation, suggesting that AzoR mediated intermicrobial communication to promoted lycopene synthesis during interspecies communication. This work provided new strategies for microbial communication monitoring and biomanufacturing. Subsequently, they developed a bispecific metabolic monitoring platform for bacterial identification and antibiotic sensitivity testing (Figure 5B) [73]. Two core-shell PLNPs with surface-confined red and green PersL were designed and functionalized with BHQ-3 energy receptor, showing amplified FRET efficiency through surface confinement effects. Extracellular bacteria (AzoR and lipase) could catalyze the reductive cleavage of azo bonds in BHQ-3 and recover the PersL. Different bacteria exhibited characteristic red/green emission patterns due to differences in enzyme expression and secretion. Machine learning models were trained to analyze the emission patterns, enabling bacterial identification with an overall accuracy of 100%. This model could also distinguish between active and inactive states of bacteria

after antibiotic treatment, enabling rapid antibiotic sensitivity testing and providing new strategies for infection treatment and bacterial communication monitoring.

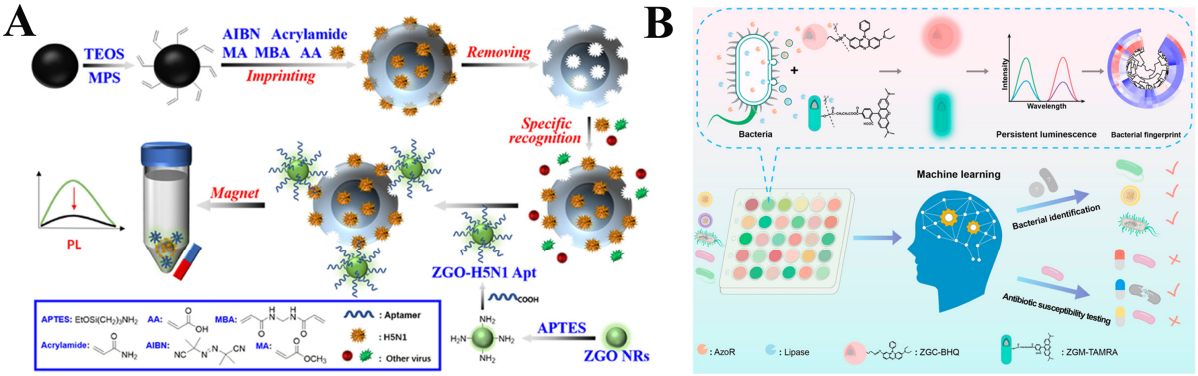


Figure 5. (**A**) Principle of the preparation of the MIP-aptasensor. Reprinted with permission from ref. [71]. Copyright 2022, American Chemical Society. (**B**) Bacterial identification and antibiotic susceptibility testing based on the machine learning-aided bispecific metabolic monitoring platform. Reprinted with permission from ref. [73]. Copyright 2025, American Chemical Society.

4.4. Metal Ions and Small Molecule Sensing

In the field of heavy metal ion detection, InPLNPs stand out for their sustained emission after excitation ceases. By virtue of time-resolved detection techniques, they effectively eliminate matrix autofluorescence interference and markedly enhance detection accuracy in complex samples. A PersL nanobeacon based on Zn_2GeO_4:Mn nanorods and Pb^{2+}-specific DNAzyme was developed for Pb^{2+} detection [76]. It retained high signal-to-background ratios in real samples, outperforming fluorescent assays, and could be adapted to other DNAzyme-specific ions. For Cd^{2+} detection, two aptamer-based sensing platforms have been established via PLRET mechanism. One was an "off-on" aptasensor [77], in which BHQ_1-labeled complementary DNA initially quenched the luminescence. Target Cd^{2+} triggered aptamer conformational rearrangement to restore the signal, enabling reliable detection in drinking water and yesso scallop samples. The other adopted an "on-off" design combined with magnetic separation, which streamlined sample pretreatment and achieved a limit of detection as low as 0.04 ng mL^{-1}, well suited for complex food matrices [78]. Ge et al. [79] developed a NIR PersL probe based on the inner filter effect (IFE) for As(III) detection, using dithiothreitol-functionalized gold nanorods as quenchers. The specific interaction between As(III) and thiol groups reversed PersL quenching, allowing highly selective detection of trace As(III) in aqueous samples. Collectively, these versatile response strategies offer promising solutions for heavy metal monitoring in environmental and food safety scenarios.

Reactive oxygen species (ROS) are core regulators of cellular redox homeostasis, and their abnormal expression is closely related to various pathological processes such as inflammation, tumors, and neurodegenerative diseases. The zero-background characteristic of PersL probes offers a promising approach for their precise monitoring. Yang et al. [80] fabricated uniform ZGGO PersL nanocubes with 3.7-fold enhanced luminescence via nonstoichiometric reactions. Benefiting from H_2O_2-triggered PersL quenching via charge transfer, the ZGGO nanocubes enable autofluorescence-free serum H_2O_2 detection and glucose oxidase activity sensing. Zhang et al. [81] developed ferrocene (Fc)-functionalized ZGGO:Cr PersL nanoprobes for early diagnosis of drug-induced liver injury (DILI). Initially, the nanoprobes remained in a luminescence-quenched "off" state via energy transfer to Fc tethered by single-stranded DNA. Upon encountering hepatic H_2O_2 in DILI, the Fenton reaction produced hydroxyl radicals to cleave DNA linkers, dissociating Fc and switching on PersL (Figure 6). In an acetaminophen-induced mouse DILI model, the probe delivered a signal-to-noise ratio of 20.9 and detected injury ~10 h earlier than standard serum tests. Xie et al. [82] extended the autofluorescence-free ROS detection to early rheumatoid arthritis (E-RA) diagnosis, leveraging ROS as an early molecular biomarker that precedes radiological damage. Glutathione (GSH)-modified ultra-small $ZnGa_2O_4$:Cr^{3+} PLNPs were engineered as smart probes. Excess ROS in inflamed synovium oxidized surface thiol groups of GSH to form disulfide cross-links, driving nanoparticle aggregation and prolonged lesion retention. In collagen-induced arthritis mice, the probe achieved a 1.9-fold signal-to-noise ratio elevation in paws, outperforming micro-CT in identifying early lesions. GSH detection has been demonstrated using nanozyme-coupled PersL strategies. Chen et al. [56] developed dual-responsive persistent luminescence nanoflowers for GSH detection and imaging. MnO_2 nanozymes effectively quenched the PersL of InPLNPs, while GSH restored PersL signals by reducing MnO_2, enabling sensitive detection of GSH in biological samples [58].

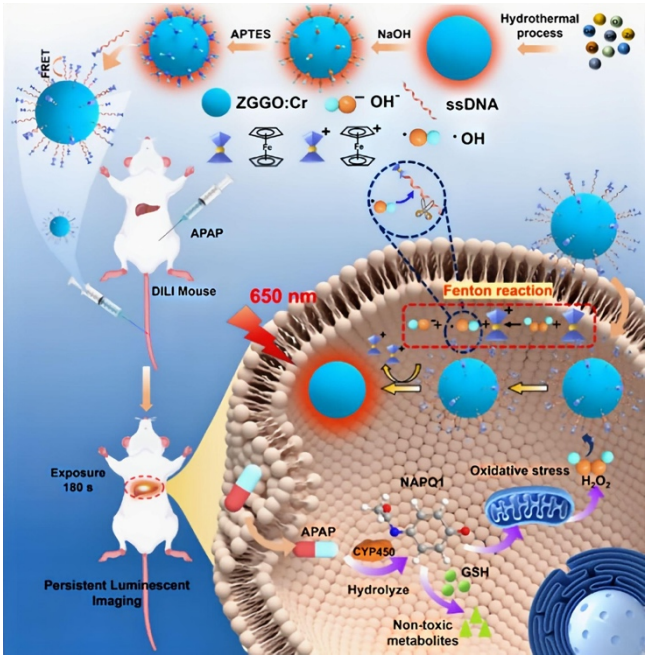


Figure 6. Schematic illustration of H_2O_2-responsive NIR PLNPs for diagnosis of DILI *in vivo*. Reprinted with permission from ref. [81]. Copyright 2025, American Chemical Society.

Beyond extrinsic surface-modified responsive systems, intrinsic pH-responsive PLNPs offered a label-free sensing strategy. Li et al. first reported acid-decomposable Zn_2GeO_4:Mn^{2+}, Pr^{3+} nanoparticles, and integrated them with enzyme-catalyzed pH modulation for autofluorescence-free glucose and aflatoxin B_1 detection as well as high-level information encryption [14]. Ma et al. further optimized this system with Eu^{3+} doping, realizing sensitive glucose assay in human serum, whole blood and urine, plus fingerprint encryption applications [83].

4.5. POCT

Point-of-care testing (POCT) enables rapid, on-site medical diagnosis, providing immediate results that support timely clinical decisions, particularly in resource-limited settings. Immunochromatographic test strip is one of the most representative POCT platforms. Replacing traditional gold nanoparticles and fluorescent microspheres with PLNPs as luminescent report probes can significantly improve the detection sensitivity of LFAs. Zhang Group developed two different PLNP-based immunochromatographic assays that eliminate autofluorescence interference by separating excitation from detection [16,84]. The first study employed NIR PLNPs for detecting the cardiac biomarker N-terminal pro-brain natriuretic peptide (NT-proBNP), achieving a detection limit of 15.28 pg/mL with 94 to101% recovery in human serum and strong correlation with the clinical gold-standard Roche electrochemiluminescence assay. The second study used green-emitting ZGM: Mn^{2+} PLNPs for dual-mode detection of heparin-binding protein (HBP), enabling both immediate visual readout under UV excitation (25 ng/mL) and ultra-sensitive PersL detection (4.7 ng/mL) without background interference (Figure 7A). Together, these PLNP-based strategies significantly enhance the sensitivity and reliability of immunochromatographic POCT, offering great promise for early disease diagnosis and on-site monitoring.

Besides, Gong et al. [85] presented a portable paper-based virus molecularly imprinted sensor for simultaneous detection of H5N1 and Hepatitis B Virus (HBV) with aptamer-functionalized PLNPs serving as signal probes (Figure 7B), thus eliminating background fluorescence by separating excitation from detection. The imprinted cavities on the paper substrate and the PLNP probes formed a sandwich-type double recognition mechanism, ensuring high specificity. The detection limits reached 16.0 aM for H5N1 and 129 fM for HBV. The low-cost, portable paper sensor enabled visual semiquantitative detection with the naked eye, avoiding expensive instruments and reducing virus spread risk from crowded testing sites.

4.6. Summary of Analytical Performance

To enable meaningful quantitative comparison across the studies reviewed, we summarize the key analytical parameters of representative InPLNP-based sensors in Table 4. This table summarizes the target analyte, InPLNP composition, recognition element, transduction mechanism, and corresponding quantitative sensing performance, including linear range, LOD, assay time, recovery, and real sample validation.

Table 4. Analytical performance of representative InPLNP-based sensors.

Target Analyte	InPLNP Composition	Recognition Element	Transduction Mechanism	Linear Range	LOD	Assay Time	Real Sample	Recovery (%)	Reference
OTA	Dual-color PLNPs	Aptamer	Ratiometric PLRET	0.01–50 ng/mL	3.4 pg/mL	50 min	Grain	97.6–105.2	[61]
AFB1	Dual-emissive PLNPs	Aptamer	Ratiometric	0.05–70 ng/mL	0.016 ng/mL	40 min	Grain	95.1–106.5	[63]
CBZ	ZGM:Mn	Aptamer + MB	Ratiometric PLRET	2.27–500 ng/mL	0.682 ng/mL	55 min	Fruit/vegetable	90.1–107.4	[39]
beta-HCH	ZGO:Mn	LinB enzyme	Competitive enzyme	0.05–14 ng/mL	0.02 ng/mL	45 min	Vegetable	88–105.3	[65]
BPA	ZGGO	Aptamer	PLRET	1–1000 ng/mL	0.27 ng/mL	2 h	Aquatic products	85.2–101.6	[54]
microRNA21	ZGO:Mn	Molecular beacon	PLRET	0.1–10 nM	0.1 nM	1 h	Serum/lysate	88.5–103.3	[12]]
PSA	ZGO:Mo	Aptamer	PLRET	10 pg/mL–10 ng/mL	9.2 pg/mL	5 h	Serum	95.8–99.1	[67]
PSA + CEA	ZGO:Mn + ZGC	Aptamer	Dual-channel PLRET	10 fg/mL–1 ng/mL (PSA), 100 fg/mL–10 ng/mL (CEA)	8.9 fg/mL (PSA), 72 fg/mL (CEA)	5 h	Serum	96.2–104.8 (PSA), 97.6–105.6 (CEA)	[68]
H5N1 virus	ZGO:Mn	MIP + Aptamer	Dual recognition	0.0128–1.28 HAU/mL	0.0128 HAU/mL	2 h	Serum	93.77–105.0	[71]
SARS-CoV-2 biomarkers	Rare-earth ions doped/co-doped $CdSiO_3$	Antibody	Lifetime/color encoding	1−200 ng/L (IgG), 1−200 ng/L (IgM), 1−100 nM (ORF1ab), 1−100 nM (RdRp), 1−100 nM (E)	Sub-nM	140 min	Serum	–	[70]
Pb^{2+}	ZGO:Mn	DNAzyme	Nanobeacon	0.5–20 nM	0.51 nM	35 min	Water	–	[76]
Cd^{2+}	ZGO:Mn	Aptamer	PLRET off-on	0.5–50 μg/L	0.35 μg/L	25 min	Water/seafood	104–107	[77]
NT-proBNP	ZGSO:Cr,Y	Antibody	LFA	15.28–9000 pg/mL	15.28 pg/mL	15 min	Serum	93.6–101	[84]
HBP	ZGM:Mn	Antibody	Dual-mode LFA	0–350 ng/mL	4.7 ng/mL	20 min	Serum	–	[16]

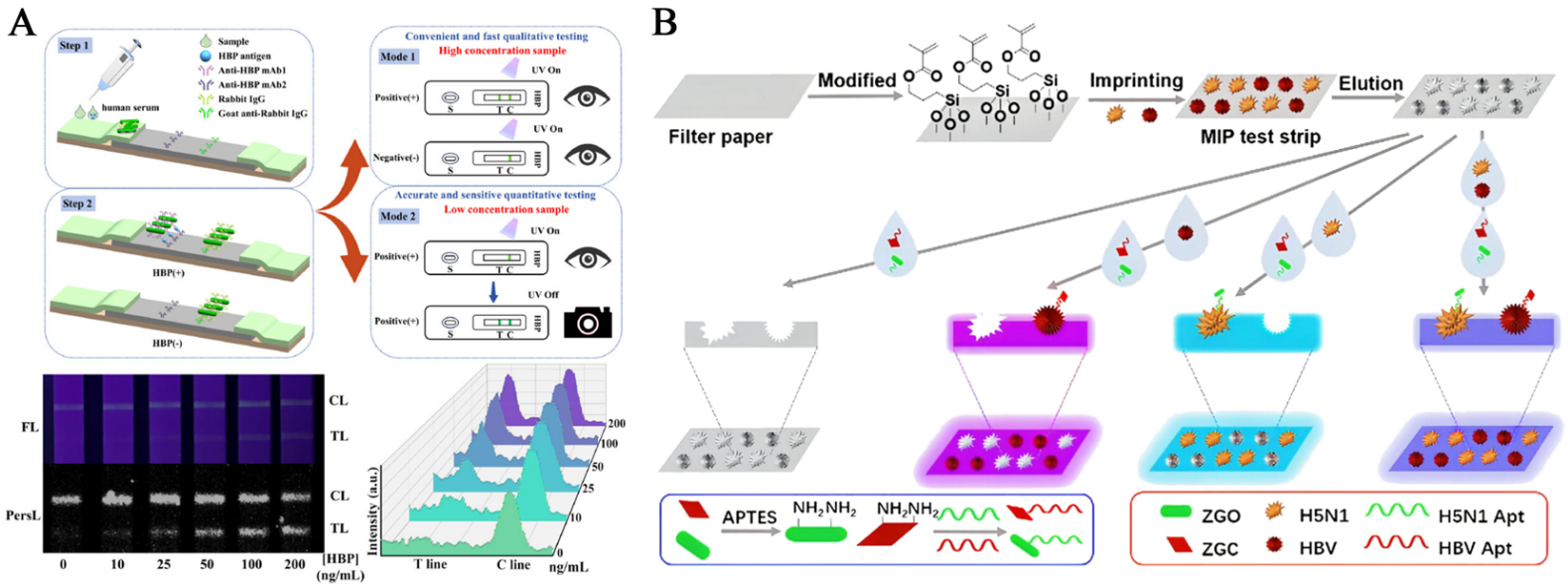


Figure 7. (**A**) Schematic diagram of the principle of HBP detection by ZGM immunochromatographic test paper. Reprinted with permission from ref. [16]. Copyright 2024, American Chemical Society. (**B**) Preparation and detection principle of the sensor. Reprinted with permission from ref. [85]. Copyright 2023, American Chemical Society.

5. Summary and Outlook

This review has surveyed the current landscape of InPLNPs for sensing and detection, benchmarking host-matrix systems, nanoscaling synthesis and surface functionalization, PersL mechanisms and performance-regulation strategies, as well as the principal sensing architectures built on capture-enrichment, PLRET, ratiometric, and nanozyme-coupling principles. Across food safety, environmental monitoring, biomarker analysis, pathogen detection, and point-of-care testing, InPLNPs have matured into a promising optical sensing platform. Yet the path from proof-of-concept demonstrations to reliable, deployable sensors remains obstructed by interconnected challenges spanning materials science, metrology, and regulatory science.

Batch-to-batch reproducibility is arguably the foremost barrier. Since PersL performance depends on subtle lattice defects and dopant distributions, nominally identical syntheses often yield probes with markedly different brightness and decay kinetics. Quantitative trap characterization, including depth-resolved thermoluminescence, trap-density quantification, and standardized decay-kinetics reporting, is still not routinely applied to trace these variations, so defect engineering continues to rely on empirical co-doping recipes rather than on measured trap distributions. Standardized synthesis protocols, quality-control metrics (particle size, dopant homogeneity, PersL brightness and lifetime), and scalable routes reproducible at gram scale are therefore essential to suppress batch variability, lower manufacturing cost, and advance probes from bespoke laboratory batches to commercial reagents. Only reproducible and economical production will allow InPLNP sensors to be benchmarked and adopted beyond individual laboratories.

Metrology and lifecycle management are equally pressing. Because afterglow brightness and lifetime are currently reported under inconsistent charging conditions, integration windows, and units, cross-study benchmarking is difficult. We therefore advocate standardized reference metrics, such as calibrated photon counts or quantum yields measured against certified phosphor references, well-defined charging dose and delay/integration times. Standardized detection protocols, covering probe concentration, charging time, time-gated acquisition, and data analysis, would make literature results auditable and reproducible across groups. Likewise, matrix effects from serum, food extracts and environmental ions must be systematically evaluated through recovery and interference assays on representative real samples.

Extending PersL into the NIR-II window (1000–1700 nm), where reduced scattering and absorption would improve penetration, remains a priority *in vivo* use, although NIR-II InPLNP hosts with sufficient brightness are still scarce. Enabling deep-tissue recharging via X-ray or NIR light further promises long-term *in vivo* monitoring, yet repeated charging delivers an accumulated radiation or photothermal dose whose safety must be quantified and kept within established limits. Besides, long-term colloidal stability, probe shelf life, biosafety, and degradation/clearance pathways also demand systematic investigation through pharmacokinetic, biodistribution, and histopathological studies. A clear understanding of how these probes are eliminated, and at which doses they remain biocompatible, is essential for regulatory acceptance and clinical adoption.

Finally, practical adoption hinges on multiplexed sensing, portable instrumentation, and clinical translation. Although lifetime- and color-encoding strategies have been demonstrated, channel crosstalk from overlapping emission bands, decay interference, and cross-reactive recognition must be quantified and minimized before multiplexed panels are clinically reliable. On the instrumentation side, compact, low-cost and smartphone-based readers, including battery-operated formats for resource-limited settings, are needed for point-of-care and field deployment. Finally, validation on well-characterized clinical cohorts against gold-standard assays will determine whether these sensors reach routine use. We believe that resolving these challenges will be decisive in realizing the full potential of InPLNP-based sensing for clinical diagnosis and on-site environmental monitoring.

Author Contributions

M.C.: conceptualization, literature search, writing—original draft preparation; Y.M.: literature screening, software, data curation; L.L.: supervision, writing—reviewing and editing. All authors have read and agreed to the published version of the manuscript.

Funding

This work was financially supported by the National Natural Science Foundation of China (22074066).

Institutional Review Board Statement

Not applicable.

Informed Consent Statement

Not applicable.

Data Availability Statement

The data that support the findings of this study are available from the corresponding author.

Conflicts of Interest

The authors declare no conflict of interest.

Use of AI and AI-Assisted Technologies

No AI tools were utilized for this paper.

References

1. Deng, K.; Chen, K.; Huang, S.; et al. Research Progress of Persistent Luminescence Nanoparticles in Biological Detection Imaging and Medical Treatment. *Materials* **2025**, *18*, 3937. https://doi.org/10.3390/ma18173937.
2. Sun, S.K.; Wang, H.F.; Yan, X.P. Engineering Persistent Luminescence Nanoparticles for Biological Applications: From Biosensing/Bioimaging to Theranostics. *Acc. Chem. Res.* **2018**, *51*, 1131–1143. https://doi.org/10.1021/acs.accounts.7b00619.
3. Zhang, J.; Wang, Z.; Huo, X.; et al. Anti-Counterfeiting Application of Persistent Luminescence Materials and Its Research Progress. *Laser Photonics Rev.* **2024**, *18*, 2300751. https://doi.org/10.1002/lpor.202300751.
4. Lv, Y.; Li, C.; Zhao, N.; et al. Synergistic Energy Transfer and Electron-Capture Competition for Giant Enhancement of Red Persistent Luminescence in $LiYGeO_4:Mn^{2+}$ via Bi^{3+} Doping. *Adv. Funct. Mater.* **2026**, *36*, e11845. https://doi.org/10.1002/adfm.202511845.
5. le Masne de Chermont, Q.; Chanéac, C.; Seguin, J.; et al. Nanoprobes with Near-Infrared Persistent Luminescence for *in Vivo* Imaging. *Proc. Natl. Acad. Sci. USA* **2007**, *104*, 9266–9271. https://doi.org/10.1073/pnas.0702427104.
6. Pei, P.; Chen, Y.; Chen, X.; et al. Optothermal-Stimulated Persistent Luminescence Imaging and Therapy (OSPLIT). *Adv. Mater.* **2025**, *37*, 2500769. https://doi.org/10.1002/adma.202500769.
7. Chen, T.; Yan, D. Full-Color, Time-Valve Controllable and Janus-Type Long-Persistent Luminescence from All-Inorganic Halide Perovskites. *Nat. Commun.* **2024**, *15*, 5281. https://doi.org/10.1038/s41467-024-49654-7.
8. Deng, Z.; Zheng, D.; Zheng, L.; et al. NIR-II Afterglow Imaging: From Principles to Biomedical Applications. *Dyes Pigm.* **2026**, *254*, 113933. https://doi.org/10.1016/j.dyepig.2026.113933.
9. Gao, L.; Liu, Y.; Su, J.; et al. Modulation of Near-Infrared Afterglow Luminescence in Inorganic Nanomaterials for Biological Applications. *Adv. Mater.* **2025**, *37*, 2419349. https://doi.org/10.1002/adma.202419349.
10. Luo, X.; Shi, J.; Wang, R.; et al. Near-Infrared Persistent Luminescence Nanoprobe for Early Detection of Atherosclerotic Plaque. *ACS Nano* **2024**, *18*, 6500–6512. https://doi.org/10.1021/acsnano.3c12136.
11. Kong, J.; Sun, Y.; Ge, X.; et al. A Chlorotoxin-Directed Diselenide-Bridged Tumor-Homing Persistent Luminescence Nanoprobes Mediating Inhibition of Oxidative Phosphorylation for Long-Term Near-Infrared Imaging and Therapy of Glioblastoma. *Adv. Funct. Mater.* **2023**, *33*, 2209579. https://doi.org/10.1002/adfm.202209579.
12. Wang, X.; Wang, Y.; Chen, S.; et al. A Persistent Luminescence Resonance Energy Transfer-Based Molecular Beacon Probe for the Highly Sensitive Detection of microRNA in Biological Samples. *Biosens. Bioelectron.* **2022**, *198*, 113849. https://doi.org/10.1016/j.bios.2021.113849.
13. Qiu, L.; Tan, J.; Chen, J.; et al. Autofluorescence-Free Ratiometric Temperature Monitoring with Multiple Emissive Persistent Luminescent Nanothermometers. *Anal. Bioanal. Chem.* **2026**, *418*, 2175–2191. https://doi.org/10.1007/s00216-026-06352-1.
14. Li, J.; Huang, X.; Zhao, X.; et al. pH-Responsive Torpedo-like Persistent Luminescence Nanoparticles for Autofluorescence-Free Biosensing and High-Level Information Encryption. *Angew. Chem. Int. Ed.* **2021**, *60*, 2398–2405. https://doi.org/10.1002/anie.202011553.
15. Feng, Y.; Song, H.; Deng, D.; et al. Engineering Ratiometric Persistent Luminous Sensor Arrays for Biothiols Identification. *Anal. Chem.* **2020**, *92*, 6645–6653. https://doi.org/10.1021/acs.analchem.0c00464.
16. Gao, Y.; Shi, J.; Wu, C.; et al. Functional Green-Emitting Mn^{2+}-Doped Zinc Germanate Persistent Luminescent Nanoparticles for Dual-Mode Immunochromatographic Detection. *Anal. Chem.* **2024**, *96*, 5694–5701. https://doi.org/10.1021/acs.analchem.4c00716.
17. Zhao, X.; Gao, X.M.; Gu, T.Y.; et al. Recent Advances in Stimuli-Responsive Persistent Luminescence Nanoparticles-Based Sensors. *TrAC Trends Anal. Chem.* **2023**, *168*, 117279. https://doi.org/10.1016/j.trac.2023.117279.

18. Zhao, T.; Abdurahman, R.; Aiwaili, R.; et al. Spinel-Type Persistent Luminescence Nanoparticles: From Mechanisms, Compositions to Applications. *Coord. Chem. Rev.* **2023**, *488*, 215171. https://doi.org/10.1016/j.ccr.2023.215171.
19. Chan, M.H.; Chang, Y.C. Recent Advances in Near-Infrared I/II Persistent Luminescent Nanoparticles for Biosensing and Bioimaging in Cancer Analysis. *Anal. Bioanal. Chem.* **2024**, *416*, 3887–3905. https://doi.org/10.1007/s00216-024-05267-z.
20. Luo, Q.; Wang, W.; Tan, J.; et al. Surface Modified Persistent Luminescence Probes for Biosensing and Bioimaging: A Review. *Chin. J. Chem.* **2021**, *39*, 1009–1021. https://doi.org/10.1002/cjoc.202000583.
21. Zhang, X.; Liu, Y.; Hu, P.; et al. Hydrolytic-Resistance Long-Persistent Luminescence $SrAl_2O_4:Eu^{2+}$, Dy^{3+} Ceramics for Optical Information Storage. *Adv. Funct. Mater.* **2025**, *35*, 2414872. https://doi.org/10.1002/adfm.202414872.
22. Shen, X.; Li, M.; Liu, Q.; et al. Water-Resistant $SrAl_2O_4:Eu^{2+}$, Dy^{3+} Phosphor with Extended Afterglow Duration. *Adv. Funct. Mater.* **2026**, *36*, e15541. https://doi.org/10.1002/adfm.202515541.
23. Zheng, T.; Luo, J.; Peng, D.; et al. Persistent Photoluminescence and Mechanoluminescence of a Highly Sensitive Pressure and Temperature Gauge in Combination with a 3D-Printable Optical Coding Platform. *Adv. Sci.* **2024**, *11*, 2408686. https://doi.org/10.1002/advs.202408686.
24. Wei, X.; Huang, X.; Zeng, Y.; et al. Longer and Stronger: Improving Persistent Luminescence in Size-Tuned Zinc Gallate Nanoparticles by Alcohol-Mediated Chromium Doping. *ACS Nano* **2020**, *14*, 12113–12124. https://doi.org/10.1021/acsnano.0c05655.
25. Li, Z.; Zhang, Y.; Wu, X.; et al. Direct Aqueous-Phase Synthesis of Sub-10 Nm "Luminous Pearls" with Enhanced *in Vivo* Renewable Near-Infrared Persistent Luminescence. *J. Am. Chem. Soc.* **2015**, *137*, 5304–5307. https://doi.org/10.1021/jacs.5b00872.
26. Wang, J.; Ma, Q.; Zheng, W.; et al. One-Dimensional Luminous Nanorods Featuring Tunable Persistent Luminescence for Autofluorescence-Free Biosensing. *ACS Nano* **2017**, *11*, 8185–8191. https://doi.org/10.1021/acsnano.7b03128.
27. Cai, G.; Seguin, J.; Naillon, T.; et al. Chromium-Doped Zinc Gallate: Impact of Sn^{4+} Co-Doping on the Persistent Luminescence Properties at the Nanoscale Applied to Bio-Imaging. *Chem. Eng. J.* **2024**, *490*, 151643. https://doi.org/10.1016/j.cej.2024.151643.
28. Abdukayum, A.; Chen, J.T.; Zhao, Q.; et al. Functional near Infrared-Emitting Cr^{3+}/Pr^{3+} Co-Doped Zinc Gallogermanate Persistent Luminescent Nanoparticles with Superlong Afterglow for *in Vivo* Targeted Bioimaging. *J. Am. Chem. Soc.* **2013**, *135*, 14125–14133. https://doi.org/10.1021/ja404243v.
29. Wang, J.; Ma, Q.; Hu, X.X.; et al. Autofluorescence-Free Targeted Tumor Imaging Based on Luminous Nanoparticles with Composition-Dependent Size and Persistent Luminescence. *ACS Nano* **2017**, *11*, 8010–8017. https://doi.org/10.1021/acsnano.7b02643.
30. Paterson, A.S.; Raja, B.; Garvey, G.; et al. Persistent Luminescence Strontium Aluminate Nanoparticles as Reporters in Lateral Flow Assays. *Anal. Chem.* **2014**, *86*, 9481–9488. https://doi.org/10.1021/ac5012624.
31. Feng, Y.; Liu, R.; Zhang, L.; et al. Raspberry-like Mesoporous $Zn_{1.07}Ga_{2.34}Si_{0.98}O_{6.56}:Cr_{0.01}$ Nanocarriers for Enhanced Near-Infrared Afterglow Imaging and Combined Cancer Chemotherapy. *ACS Appl. Mater. Interfaces* **2019**, *11*, 44978–44988. https://doi.org/10.1021/acsami.9b18124.
32. Lv, X.; Chen, N.; Wang, J.; et al. Facile Thermal Decomposition Synthesis of Sub-5 Nm Nanodots with Long-Lived Luminescence for Autofluorescence-Free Bioimaging. *Sci. China Mater.* **2020**, *63*, 1808–1817. https://doi.org/10.1007/s40843-020-1339-8.
33. Wei, G.; Wang, C.; Wei, H.; et al. Enabling Persistent Luminescence of Eu^{3+} in Nanoparticles through Interfacial Energy Transfer for Advanced X-Ray Imaging. *Nano Lett.* **2025**, *25*, 6302–6309. https://doi.org/10.1021/acs.nanolett.5c01138.
34. Zou, R.; Huang, J.; Shi, J.; et al. Silica Shell-Assisted Synthetic Route for Mono-Disperse Persistent Nanophosphors with Enhanced *in Vivo* Recharged Near-Infrared Persistent Luminescence. *Nano Res.* **2017**, *10*, 2070–2082. https://doi.org/10.1007/s12274-016-1396-z.
35. Jiang, X.; Gao, X.; Li, L.; et al. Enhancement of Light and X-Ray Charging in Persistent Luminescence Nanoparticle Scintillators $Zn_2SiO_4:Mn^{2+}$, Yb^{3+}, Li^{+}. *ACS Appl. Mater. Interfaces* **2023**, *15*, 21228–21238. https://doi.org/10.1021/acsami.3c00664.
36. Zhang, Z.; Yan, H.; Qiu, B.; et al. Persistent Luminescence-Based Theranostics for Real-Time Monitoring and Simultaneously Launching Photodynamic Therapy of Bacterial Infections. *Small* **2022**, *18*, 2200813. https://doi.org/10.1002/smll.202200813.
37. Liu, J.; Kotrchová, L.; Lécuyer, T.; et al. Coating Persistent Luminescence Nanoparticles with Hydrophilic Polymers for *in Vivo* Imaging. *Front. Chem.* **2020**, *8*, 584114. https://doi.org/10.3389/fchem.2020.584114.
38. Sodia, T.Z.; Tetu, H.L.; Saccomano, S.C.; et al. Persistent Luminescence Nanosensors: A Generalized Optode-Based Platform for Autofluorescence-Free Sensing in Biological Systems. *ACS Sens.* **2024**, *9*, 3307–3315. https://doi.org/10.1021/acssensors.4c00653.

39. Zhao, X.; Qin, X.B.; Yan, Z.Y.; et al. Complementary Strand-Free Persistent Luminescence Ratiometric Aptasensor for Ultrasensitive and Selective Carbendazim Assay. *ACS Sens.* **2026**, *11*, 2807–2816. https://doi.org/10.1021/acssensors.5c04924.
40. Liang, L.; Chen, J.; Shao, K.; et al. Controlling Persistent Luminescence in Nanocrystalline Phosphors. *Nat. Mater.* **2023**, *22*, 289–304. https://doi.org/10.1038/s41563-022-01468-y.
41. Yang, L.; Gai, S.; Ding, H.; et al. Recent Progress in Inorganic Afterglow Materials: Mechanisms, Persistent Luminescent Properties, Modulating Methods, and Bioimaging Applications. *Adv. Opt. Mater.* **2023**, *11*, 2202382. https://doi.org/10.1002/adom.202202382.
42. Liu, J.; Wang, Y.; Liu, F.; et al. Recent Studies of Defects in Persistent Luminescent Materials. *Adv. Funct. Mater.* **2026**, *36*, e16560. https://doi.org/10.1002/adfm.202516560.
43. Liu, N.; Chen, X.; Sun, X.; et al. Persistent Luminescence Nanoparticles for Cancer Theranostics Application. *J. Nanobiotechnology* **2021**, *19*, 113. https://doi.org/10.1186/s12951-021-00862-z.
44. Huang, L.; Xue, M.; Wei, Y.; et al. Improving Persistent Luminescence by Defect Engineering. *Coord. Chem. Rev.* **2026**, *546*, 217088. https://doi.org/10.1016/j.ccr.2025.217088.
45. Li, Y.; Gecevicius, M.; Qiu, J. Long Persistent Phosphors—From Fundamentals to Applications. *Chem. Soc. Rev.* **2016**, *45*, 2090–2136. https://doi.org/10.1039/c5cs00582e.
46. Shi, J.; Sun, X.; Song, L.; et al. Inorganic Persistent Luminescence Materials: Emerging Optical Theranostic Agents. *Prog. Mater. Sci.* **2024**, *142*, 101246. https://doi.org/10.1016/j.pmatsci.2024.101246.
47. Parayil, R.T.; Gupta, S.K.; Mohapatra, M. A Review on Defect Engineered NIR Persistent Luminescence through Transition Metal Ion (Cr, Mn, Fe and Ni) Doping: Wider Perspective Covering Synthesis, Characterization, Fundamentals and Applications. *Coord. Chem. Rev.* **2025**, *522*, 216200. https://doi.org/10.1016/j.ccr.2024.216200.
48. Qi, B.; Dai, W.; Lou, B.; et al. Amplifying Persistent Luminescence in Heavily Doped Nanopearls for Bioimaging and Solar-to-Chemical Synthesis. *ACS Nano* **2025**, *19*, 5818–5828. https://doi.org/10.1021/acsnano.4c18244.
49. Pei, P.; Wang, L.; Jing, H.; et al. Progress and Prospects of Persistent Luminescent Nanocrystals in Biomedical Applications. *Adv. Opt. Mater.* **2026**, *14*, e03006. https://doi.org/10.1002/adom.202503006.
50. Ma, X.; Wang, Y.; Seto, T. Electrical Stimulation for Brighter Persistent Luminescence. *Light Sci. Appl.* **2024**, *13*, 165. https://doi.org/10.1038/s41377-024-01507-0.
51. Lin, C.; Yang, R.; Wu, Z.; et al. Electrically Chargeable Inorganic Persistent Luminescence in an Alternating Current Driven Electroluminescent Device. *Commun. Mater.* **2025**, *6*, 25. https://doi.org/10.1038/s43246-025-00746-x.
52. Wei, Y.; Song, M.; Li, L.; et al. Enhanced Long-Lasting Luminescence Nanorods for Ultrasensitive Detection of SARS-CoV-2 N Protein. *Sci. China Mater.* **2025**, *68*, 253–260. https://doi.org/10.1007/s40843-024-3148-9.
53. Feng, Y.; Yang, X.; Rao, Q.; et al. Persistent Luminescence Lifetime-Based Near-Infrared Nanoplatform via Deep Learning for High-Fidelity Biosensing of Hypochlorite. *Anal. Chem.* **2024**, *96*, 7240–7247. https://doi.org/10.1021/acs.analchem.4c00899.
54. Zhang, L.W.; Yan, Z.Y.; Zhao, X.; et al. Undoped Zinc Gallogermanate Nanoparticles Based Persistent Luminescence Aptasensor for the Determination of Bisphenol a in Aquatic Products. *Spectrochim. Acta Part A Mol. Biomol. Spectrosc.* **2026**, *352*, 127553. https://doi.org/10.1016/j.saa.2026.127553.
55. Li, L.; Geng, P.; Huo, M.; et al. Persistent Luminescence Ratiometric Thermometry at the Nanoscale. *Adv. Opt. Mater.* **2025**, *13*, e02186. https://doi.org/10.1002/adom.202502186.
56. Chen, X.; Zhang, H.; Liang, X.; et al. Dual-Responsive Persistent Luminescence Nanoflowers for Glutathione Detection and Imaging. *Sens. Actuators B Chem.* **2024**, *403*, 135200. https://doi.org/10.1016/j.snb.2023.135200.
57. Zhu, Y.; Wen, Y.; Xie, Y.; et al. Intelligent Hierarchical Targeting Near-Infrared Persistent Luminescence Nanosystem for Improved Nuclear Delivery and Simultaneous Visualization/Therapy of EBV-Associated Cancer. *ACS Appl. Mater. Interfaces* **2025**, *17*, 3072–3083. https://doi.org/10.1021/acsami.4c20023.
58. Zhang, Y.; Abdurahman, R.; Zhang, R.; et al. Intelligent Paper Chip Sensor Based on MnO_2 Nanozyme@Persistent Luminescent Nanoparticles for Trimodal Detection of Glutathione. *Microchem. J.* **2025**, *208*, 112343. https://doi.org/10.1016/j.microc.2024.112343.
59. Zhang, Y.; Zhou, J.; Zhang, X.X.; et al. NIR Persistent Luminescence Nanoparticles Based Turn-on Aptasensor for Autofluorescence-Free Determination of 17β-Estradiol in Milk. *Food Chem.* **2022**, *373*, 131432. https://doi.org/10.1016/j.foodchem.2021.131432.
60. Wang, B.B.; Zhao, X.; Chen, L.J.; et al. Functionalized Persistent Luminescence Nanoparticle-Based Aptasensor for Autofluorescence-Free Determination of Kanamycin in Food Samples. *Anal. Chem.* **2021**, *93*, 2589–2595. https://doi.org/10.1021/acs.analchem.0c04648.
61. Guo, J.X.; Pan, L.M.; Wang, M.C.; et al. Exogenous Interference and Autofluorescence-Free Ratiometric Aptasensor for Detection of OTA Based on Dual-Colored Persistent Luminescence Nanoparticles. *Food Chem.* **2023**, *413*, 135611. https://doi.org/10.1016/j.foodchem.2023.135611.

62. Jiang, Y.Y.; Zhao, X.; Chen, L.J.; et al. Persistent Luminescence Nanorod Based Luminescence Resonance Energy Transfer Aptasensor for Autofluorescence-Free Detection of Mycotoxin. *Talanta* **2020**, *218*, 121101. https://doi.org/10.1016/j.talanta.2020.121101.
63. Pan, L.M.; Zhao, X.; Wei, X.; et al. Ratiometric Luminescence Aptasensor Based on Dual-Emissive Persistent Luminescent Nanoparticles for Autofluorescence- and Exogenous Interference-Free Determination of Trace Aflatoxin B1 in Food Samples. *Anal. Chem.* **2022**, *94*, 6387–6393. https://doi.org/10.1021/acs.analchem.2c00861.
64. Jiang, Y.Y.; Zhao, X.; Chen, L.J.; et al. A Dual-Colored Persistent Luminescence Nanosensor for Simultaneous and Autofluorescence-Free Determination of Aflatoxin B1 and Zearalenone. *Talanta* **2021**, *232*, 122395. https://doi.org/10.1016/j.talanta.2021.122395.
65. Xu, Q.; Zhao, X.; Chen, L.J.; et al. Persistent Luminescence-Based Competitive Enzyme Biosensor for Ultrasensitive and Selective Detection of β-Hexachlorocyclohexane. *Anal. Chem.* **2026**, *98*, 13897–13903. https://doi.org/10.1021/acs.analchem.6c01520.
66. Yan, Z.Y.; Yuan, L.; Hao, F.; et al. Autofluorescence-Free Sensing of Released Bisphenol a from Packaging Materials by a Persistent Luminescence Aptasensor. *Anal. Chem.* **2025**, *97*, 22145–22152. https://doi.org/10.1021/acs.analchem.5c04090.
67. Zhao, Y.; Zheng, F.; Shi, L.; et al. Autoluminescence-Free Prostate-Specific Antigen Detection by Persistent Luminous Nanorods and Au@Ag@SiO_2 Nanoparticles. *ACS Appl. Mater. Interfaces* **2019**, *11*, 40669–40676. https://doi.org/10.1021/acsami.9b14901.
68. Shi, L.; Shao, J.; Jing, X.; et al. Autoluminescence-Free Dual Tumor Marker Biosensing by Persistent Luminescence Nanostructures. *ACS Sustain. Chem. Eng.* **2020**, *8*, 686–694. https://doi.org/10.1021/acssuschemeng.9b06621.
69. Wang, R.; Shi, J.; Wu, C.; et al. High-Sensitivity PD-L1 Immune Checkpoint Imaging in Microtumors for Immunotherapy Using Near-Infrared Persistent Luminescence Nanoparticles. *Biosens. Bioelectron.* **2026**, *292*, 118070. https://doi.org/10.1016/j.bios.2025.118070.
70. Feng, Y.; Chen, T.; Rao, Q.; et al. Time-Resolved Persistent Luminescence Encoding for Multiplexed Severe Acute Respiratory Syndrome Coronavirus 2 Detection. *Anal. Chem.* **2022**, *94*, 16967–16974. https://doi.org/10.1021/acs.analchem.2c04788.
71. Chen, S.; Cai, G.; Gong, X.; et al. Non-Autofluorescence Detection of H5N1 Virus Using Photochemical Aptamer Sensors Based on Persistent Luminescent Nanoparticles. *ACS Appl. Mater. Interfaces* **2022**, *14*, 46964–46971. https://doi.org/10.1021/acsami.2c12088.
72. Miao, Z.; Dai, W.; Jin, Y.; et al. Surface-Confined Persistent Luminescence with Amplified FRET Efficiency for Cell-Cell Communication Monitoring. *Sci. China Chem.* **2025**, *68*, 2680–2690. https://doi.org/10.1007/s11426-024-2450-6.
73. Chen, J.; Miao, Z.; Ma, C.; et al. Bispecific Metabolic Monitoring Platform for Bacterial Identification and Antibiotic Susceptibility Testing. *ACS Sens.* **2025**, *10*, 1470–1482. https://doi.org/10.1021/acssensors.4c03534.
74. Liu, Z.; Pan, J.; Tan, J.; et al. Tunable Persistent Luminescence Nanoparticles for Profiling Bacterial Extracellular Azoreductase Activity and Antibiotic Susceptibility. *Anal. Bioanal. Chem.* **2026**, *418*, 4529–4540. https://doi.org/10.1007/s00216-026-06547-6.
75. Tan, J.; Zhang, Y.; Shi, Y.; et al. Boosting Persistent Luminescence with Spatially Confined Ion Doping for Profiling Bacterial-Environment Interactions. *ACS Appl. Mater. Interfaces* **2026**, *18*, 24082–24092. https://doi.org/10.1021/acsami.6c01361.
76. Luo, Q.; Qin, L.; Zhang, P.; et al. A Persistent Luminescent Nanobeacon for Practical Detection of Lead Ions via Avoiding Background Interference. *Anal. Chim. Acta* **2022**, *1198*, 339555. https://doi.org/10.1016/j.aca.2022.339555.
77. Lai, B.; Wang, H.; Su, W.; et al. A Phosphorescence Resonance Energy Transfer-Based "off-on" Long Afterglow Aptasensor for Cadmium Detection in Food Samples. *Talanta* **2021**, *232*, 122409. https://doi.org/10.1016/j.talanta.2021.122409.
78. Lai, B.; Wang, R.; Yu, X.; et al. A Highly Sensitive "on-off" Time-Resolved Phosphorescence Sensor Based on Aptamer Functionalized Magnetite Nanoparticles for Cadmium Detection in Food Samples. *Foods* **2020**, *9*, 1758. https://doi.org/10.3390/foods9121758.
79. Ge, K.; Liu, J.; Wang, P.; et al. Near-Infrared-Emitting Persistent Luminescent Nanoparticles Modified with Gold Nanorods as Multifunctional Probes for Detection of Arsenic(III). *Microchim. Acta* **2019**, *186*, 197. https://doi.org/10.1007/s00604-019-3294-z.
80. Yang, S.; Dai, W.; Tang, M.; et al. Nonstoichiometric Nanocubes with a Controllable Morphology and Persistent Luminescence for Autofluorescence-Free Biosensing. *ACS Appl. Mater. Interfaces* **2023**, *15*, 38644–38652. https://doi.org/10.1021/acsami.3c05895.
81. Zhang, F.; Song, L.; Lin, Y.; et al. Smart Persistent Luminescence Imaging for Early Diagnosis of Drug-Induced Liver Injury. *Chem. Biomed. Imaging* **2025**, *3*, 77–84. https://doi.org/10.1021/cbmi.4c00056.
82. Xie, Y.; Zou, Q.; Zhu, Y.; et al. A Smart Ultra-Small near Infrared Persistent Luminescence Nanoprobe for Non-Invasive Detection of Early Rheumatoid Arthritis. *Colloids Surf. B Biointerfaces* **2025**, *255*, 114915. https://doi.org/10.1016/j.colsurfb.2025.114915.

83. Ma, X.; Zhu, R.; Zhang, H.; et al. pH-Responsive Persistent Luminescence Nanoprobes Biosensor for Autofluorescence-Free Determination of Glucose Level in Human Samples and Fingerprint Encryption. *Luminescence* **2024**, *39*, e4900. https://doi.org/10.1002/bio.4900.
84. Gao, Y.; Shi, J.; Sun, X.; et al. Near-Infrared Persistent Luminescence Nanoparticles-Based Immunochromatographic Assay for Autofluorescence-Free Detection. *ACS Appl. Nano Mater.* **2024**, *7*, 20820–20828. https://doi.org/10.1021/acsanm.4c03766.
85. Gong, H.; Chen, S.; Tang, L.; et al. Ultra-Sensitive Portable Visual Paper-Based Viral Molecularly Imprinted Sensor without Autofluorescence Interference. *Anal. Chem.* **2023**, *95*, 17691–17698. https://doi.org/10.1021/acs.analchem.3c03506.